Bifocal Metalens: An Investigation

Ravindu Karunathilake

Optical devices play a vital role in the modern technologies, and the desire for more efficient and high-speed computation is driving the world toward device miniaturization. This trend, first observed with the transistor, is now an aspiration for optical systems. Among the optical systems, the humble lens is an essential component. However, traditional lens designs are incompatible with nanoscale manufacturing. Metalenses are now emerging as a possible solution to this incompatibility. The optical lens made from subwavelength resonators hold promise for nanoscale integration as it provides small foot-print, and low-cost functionality. In this report, an investigation of one such device is summarized. The metalens under study uses phase change material to design a tunable metalens. The report then further extends on this design by analyzing a polarization sensitive metalens using phase change material. The extended device is able to focus light with high transmission efficiency while introducing polarization helicity conversion to incident linearly polarized light.

The development of optical lenses have revolutionized our understanding of the universe. The simple lens allowed Galileo to challenge the Aristotelian cosmological wisdom of the 17^{th} century and enabled Robert Hooke to discover the microscopic world. Today, lenses have become ubiquitous—finding applications in corrective glasses, imaging systems, microscopy, and nanofabrication to name a few.

Traditional optical lenses are engineered from either transparent or reflective media to control the path of light. Refractive lenses rely on the gradual phase accumulation along the optical path to focus the incident light. This phase is typically imparted by polishing the lens topology to shape the light rays to a tight focus.[1] The reliance on surface topology of the lens to impart this phase delay unfortunately binds the performance of the lens to the precision of the manufacturing process—greatly increasing the cost of production. Furthermore, due to material dispersion (dependence of material refractive index on the wavelength of light) different wavelengths of light is imparted different phase delays. This phenomena is known as chromatic aberration (Fig. 1a), and is an importance consideration when designing an optical system. To eliminate this type of aberration in optical systems, designers employ a cascade of achromatic lenses (Fig. 1b) in the form of doublets and triplets to create a single focus point during multi-wavelength applications.[1] This however makes the whole system more complex, bulky and costly to manufacture.

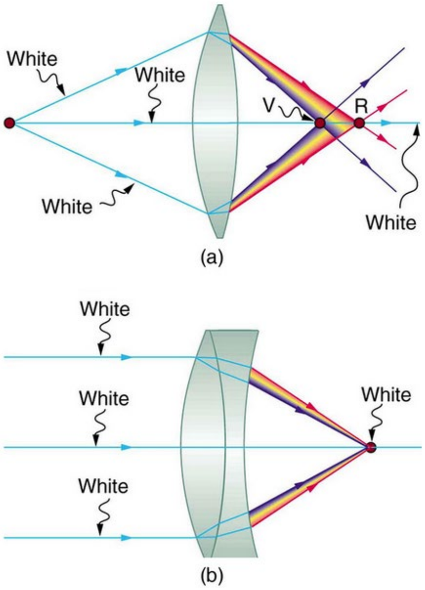

Fig.1 | Chromatic aberration in lenses. A) A diagram depicting the material dispersion of the lens creating multiple focal points of light for each wavelength present in the incident white light. B) An achromatic doublet typically used in optical systems to correct for chromatic aberration by focusing multiple wavelength of light to the same focusing point.[2]

The desire for more powerful functionality while minimizing energy consumption is leading to a miniaturization of many optical systems. This downscaling of optical devices are incompatible with the traditional large footprint designs as surface area is at a premium. An emerging technology that shows great potential in this regard are metasurface based thin optical elements. These devices are composed of subwavelength unit cells ("meta atoms") which provide a new mechanism for shaping the wavefront of light. Additionally, metasurface based flat optics (metalenses) designed using low-loss dielectrics are compatible with the modern CMOS manufacturing – dramatically reducing the cost of production.

This report details the investigation of one such device using phase change material (PCM) to realize a tunable metalens. In the begin sections of this report, an overview of metalens design will be provided along with a discussion of three main mechanisms for imparting phase delay onto the incident light. Following this introduction, a summary of the literature work under investigation[3] is provided. In addition, a detail discussion of design extension to create polarization sensitive metalens operation is given. The report concludes with an examination of literature work in the field of metalens design and a discussion of possible fabrication methods and characterization for the proposed device.

Metalens Design: Theory

As previously mentioned, just as traditional lens topology is used to impart a phase delay onto incident light based on spatial position, metalenses are able to shape a wavefront of light based on the phase delay provided by subwavelength resonators. This is accomplished by inducing a constant gradient of phase discontinuity along the metasurface interface. Through the application of generalized Fermat's principle, the generalized law of reflection and refraction (Eq. 1) describes this principle of operation.[4]

$$\sin(\theta_t)n_t - \sin(\theta_i)n_i = \frac{\lambda_0}{2\pi}\frac{d\phi}{dx} \qquad (1)$$

Where θ_t and θ_i are the angle of refraction and incidence, respectively; λ_0 is the vacuum wavelength. The term $(d\phi/dx)$ describes the gradient of phase discontinuity along the interface. The formulation of the above equation implies that a refracted beam of light may be deflected to any arbitrary angle (θ_t) given a suitable constant of phase discontinuity along the plane of incidence created between two materials with refractive index n_i and n_t (Fig. 2).

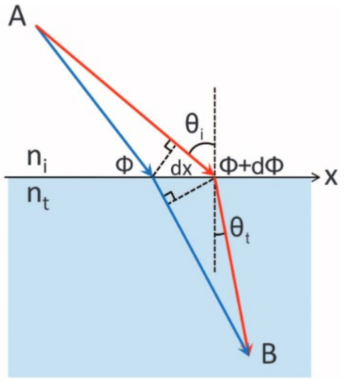

Fig. 2 | Generalized Snell's law of refraction. The diagram outlines the main principle of engineering phase discontinuity along an interface using subwavelength resonators. Two light rays originating from point 'A' is incident on the material interface described by the incident refractive index n_i and transmitted index of refraction n_t. The two rays experiences an abrupt constant gradient of phase shift at the interface which is a function of position along the interface such that both rays refract to point 'B'.[4]

The metalens design is based on engineering a hyperbolical phase profile along the interface.[5] With this approach, similar to traditional lens designs, the secondary waves emerging from the unit cells constructively interfere at the focal plane. For a lens design focal length (f), the phase $\phi(x,y)$ is mapped to every point $P_L(x,y)$ on the metalens following equation 2.[5]

$$\phi_L(x,y) = \frac{2\pi}{\lambda_0}\overline{P_L S_L} = \frac{2\pi}{\lambda_0}\left(\sqrt{(x^2+y^2)+f^2}-f\right) \quad (2)$$

A schematic showing the design of a flat lens is shown in Figure 3, where derivation of equation 2 based on simple Pythagorean principles is evident.

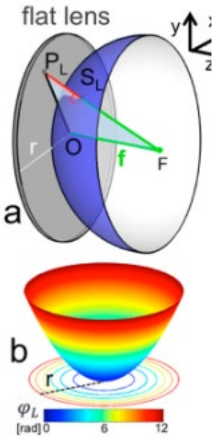

Fig. 3 | Metalens phase mapping principle. In order to emulate the focusing capability of a traditional lens, a hyperbolic phase profile must be mapped to the flat lens surface. A) The phase shift at a point $P_L(x,y)$ on the flat lens surface is proportional to the distance $\overline{P_L S_L}$, where S_L is the projection of point P_L onto the spherical surface (representing the desired phase) with radius equation to the focal length f. B) The resulting hyperbolic radial phase distribution along the flat lens surface.[5] Note however, the generated phase profile is continuous, however in practice this phase profile must be discretized since finite subwavelength dimensional resonators are used to realize the required phase delay.

In practice, these radial phase delays are achieved by three mechanisms. First the subwavelength unit cell may be treated as a truncated waveguide. Secondly, the phase delay is obtain through the orientation of the unit cell, known as geometrical phase and finally, the unit cells may be treated as a resonant subwavelength nanoantennas acting as secondary point sources. The details of these approaches are discussed in the following sections of this report.

Phase Mechanism: Waveguiding Effect

The operation principle of this approach relies on the waveguiding effects of the unit cell structures. The unit cell is typically treated as a truncated waveguide with low-quality factor Fabry-Perot resonances that interfere and lead to high transmission.[6] Using this approach, a variation in the lateral dimension of the unit cell will lead to changes in effective index which effects the propagation constant in the waveguide and in turn a different phase delay is realized (Fig. 4). However, the unit cell structure also contains dipoles, quadrupole, and higher order electric and magnetic multipole in its multipole expansion.[6] Furthermore, effective medium method fails to capture the underlying physics of periodic structures supporting multiple modes. As would be the case for most unit cells structures in a typical metalens design. Therefore, relying solely on the waveguiding effect to design metalens phase profiles would not be adequate.

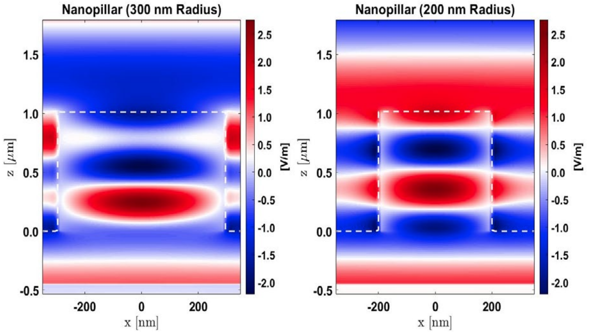

Fig. 4 | Electric field maps for truncated circular waveguide pillars. As seen from the field profiles, there is a clear phase difference between the 300 nm (left) pillar structure and the 200 nm (right) pillar. By treating this structure as a truncated waveguide, this effect is attributed to the modal effective index changes as a result of variations in the transverse dimensions – altering the mode profiles within the waveguide.

Phase Mechanism: Geometrical Phase

Another approach for imparting phase delay is geometrical phase, which is also known as Pancharatnam-Berry phase. This mechanism relies not on the dimensional variations of the unit cell, but the azimuthal orientation of the unit cell on the metasurface. One such geometric metasurface working in the transmission mode based on silicon structures is shown in Figure 5. The design uses subwavelength spaced silicon nanostripes as unit cell structures, which imparts a phase difference of π for light of orthogonal polarizations. In this mechanism, the acquired phase delay is independent of subwavelength structural dimensions, resonances, and material properties. As such, this approach is desirable for wideband operations such as in imaging applications. However, to utilize this approach requires radially asymmetric structures, which gives the designed lens an inherent polarization sensitivity. This sensitivity may not be appropriate for all applications.

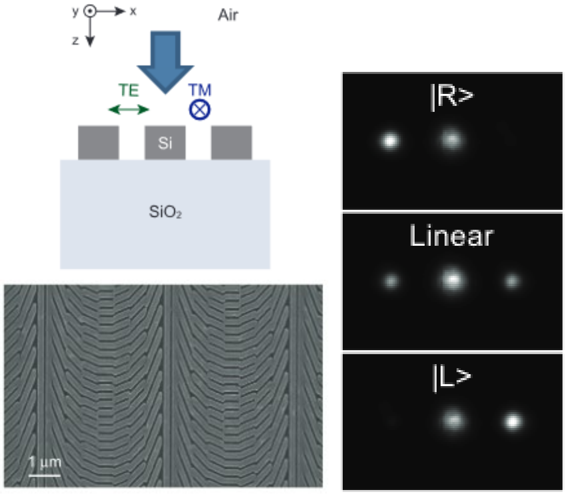

Fig. 5 | All-dielectric metasurface utilizing geometrical phase. The figure contains an SEM image of the metasurface using geometrical phase to control the diffraction pattern for right circular polarization (top), linear polarization (middle), and left circular polarization (bottom) at 550 nm.[8]

Phase Mechanism: Huygens Nanoantennas

Christiaan Huygen theorized that every point on a wavefront can be treated as a secondary source of outgoing waves. Then, Love showed these secondary sources may be described as electrically small antennas that radiate the crossed electric and magnetic dipoles.[9] These sources can be created by utilizing the strong electric and magnetic resonances of high-permittivity all-dielectric antennas. As such, these resonances may be altered via unit cell geometry to tailor the scattering cross section of the individual structures. This approach provides the full 2π phase needed in metalens design while allowing for high transmission efficiency.[9] The origin of this approach lies in Mie theory where spherical particles with high-permittivity in general feature both electric and magnetic resonances.[7] Furthermore, since the conclusions of Mie theory are valid for any arbitrary shaped nanoparticle, the subwavelength nanoantennas (or unit cells) should also possess this response. Moreover, by the careful tuning of structural parameters, it is possible to spectrally overlap (Fig. 6) electric dipole (ED) and magnetic dipole (MD) of equal strength, as governed by the Kerker condition, to realize strong directional scattering. Where the phase of the transmitted light is determined by the exact value of the ED and MD moments.[7]

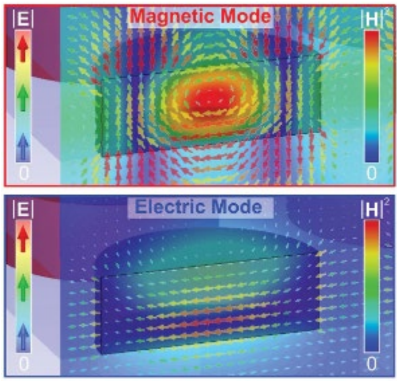

Fig. 6 | Field distribution is a silicon-nanodisk. The magnetic (top) and electric (bottom) mode of the structure is shown. These modes are dominated by strong magnetic and electric dipole moments, respectively.[9]

Work Under Investigation

The literature work that is the subject of this report concerns with the design of an all-dielectric metalens with germanium antimony telluride (GST) phase change material integration. The proposed metalens operates in the near-infrared (NIR) region (1550 nm) with two focal points. The presented design is an active metasurface in the sense that modulation of focusing intensity between to two foci are possible. This tunability of the metalens is a direct result of the phase transition capabilities of GST material.[10]

Phase-change materials have widely been used in optical disks and electronic memory due to their nonvolatile transition between the amorphous (a-GST) and crystalline (c-GST) states under a stimulus: thermal, optical and electrical.[3] This phase transition is significant due to the achievement of large refractive index contrast with moderate optical losses (Fig. 7). As can be seen from the plot, GST showcases moderate optical loss at the designed wavelength of 1550 nm. Additionally, GST is commercially available, thus proven to be stable and provide large phase transitional cycles – ideal for metalens designs where longevity of the lens is a vital design consideration.

The proposed metasurface is designed on a SiO_2 substrate consisting of radially symmetric hybrid pillar structure for a unit cell (Fig. 8). The unit cell structure consists of a bottom Si layer (300 nm) with a top GST layer (20 nm) on a square lattice with a period of 700 nm. This period was chosen as to avoid diffraction of light into non-zero diffraction orders.[3] Two focusing points are achieved via a novel spatial multiplexing scheme where the metasurface surface (29 μm by 29 μm) is divided into two regions (Fig. 9).

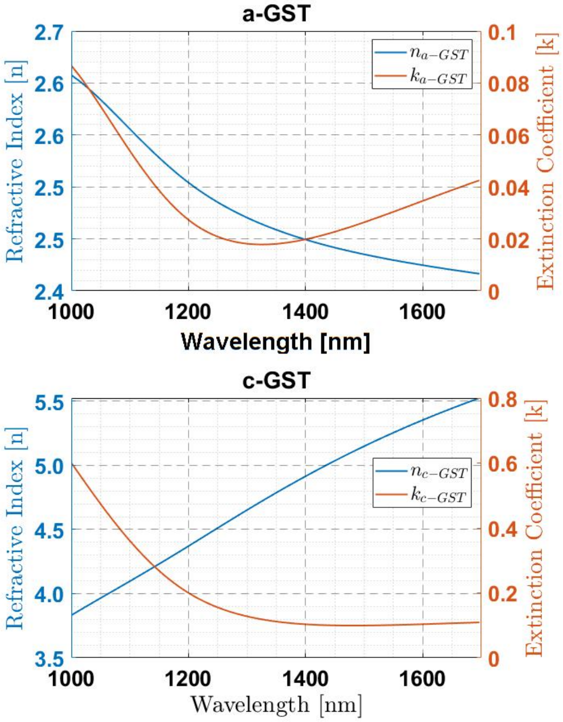

Fig. 7 | GST index data. A plot of refractive index and extinction coefficient data for GST in both amorphous and crystalline phase. Data was taken from ref.[11]

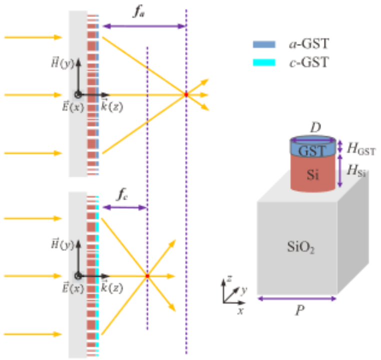

Fig. 8 | Bifocal metalens design. A schematic of a single unit cell (right) and the spatially multiplexed lens design (left) depicting the focal modulation between the amorphous (top) and crystalline (bottom).[3]

Region 1 (outer) correspond to a metalens phase profile (designed using equation 2) to focus light at a distance of 10 μm along the optical axis of the metalens. Likewise, region 2 (inner) correspond to a metalens phase profile with a focal point at 5 μm. The final metalens is comprised of 41 by 41 unit cells. The inner region consists of 19 by 19 unit cells with an area of 13 μm by 13 μm.

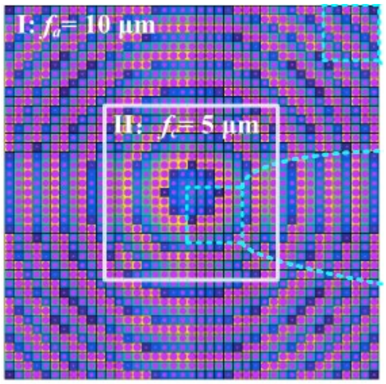

Fig. 9 | Bifocal metalens spatial multiplexing scheme. A schematic shows the bisector (white square region) diving region 1 (outer) and region 2 (inner). Region 1 consists of unit cells based on the optical response when the GST layer is in the amorphous phase. Region 2 consists of unit cells based on the optical response when the GST layer is in the crystalline phase. Both regions have 8 levels of discretization.[3]

Reproduced Results and Discussion

The metalens under investigation uses lateral unit cell structural changes to induce a phase delay onto to the incident light. Therefore, the first step in designing this metalens is to generate the phase and transmission response of the unit cell structure (Fig. 10). The spectral response was simulated using 3D finite-difference time-domain approach (Lumerical Inc. FDTD) under periodic boundary condition (BC) along the x- and y-axis, and perfectly matched layer (PML) along the z-axis (see Fig. 8 for axial orientation). Additionally, a plane-wave source polarized along the x-axis was incident in the positive z direction. The reproduced results show a high level of agreement with the results presented in the literature under investigation. The proposed unit cell is able to achieve a 2π phase response while maintaining a high level of transmission for ~72% of the pillar diameter sweep range. However, a slight blue shift in the optical response can be seen. This slight variation is attributed to a mismatch between the material index and meshing size.

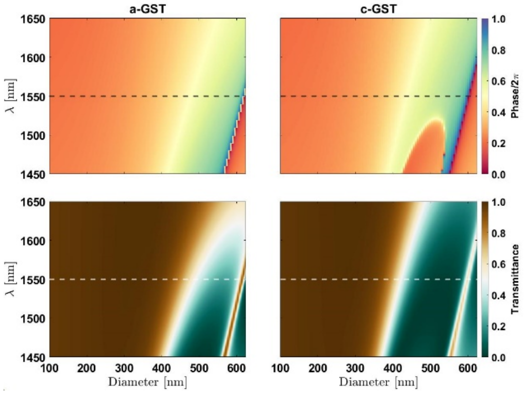

Fig. 10 | Broadband parameter sweep of the unit cell. The left column represent the normalized phase (top) and transmittance (bottom) for amorphous GST. The right column represent the normalized phase (top) and transmittance (bottom) for crystalline GST. The parameter sweep was executed in a wavelength range of 1450 nm to 1650 nm for 100 increments of the pillar diameter from 100 nm to 620 nm. The dotted horizontal lines represent the optical response at a wavelength of 1550 nm.

Due to the slight variation in optical response, the structural dimensions for the unit cell in both a-GST and c-GST where adjusted accordingly during the generation of the phase map (Fig. 11). A constant phase gradient ($d\phi/dx$) of $\pi/4$ was chosen for both a-GST and c-GST cases.

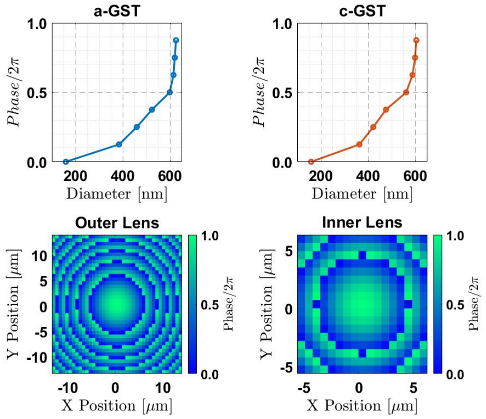

Fig. 11 | Phase maps. The left column indicates the phase discretization (top) and phase map (bottom) for the amorphous GST state. Likewise, the right column shows the discretization (top) and phase map (bottom) for the crystalline GST state. Two align with ref. [3]8 levels of discretization was employed.

After acquiring the required phase maps for realizing focal spots at 10 μm (outer) and 5 μm (inner lens) a structural map was created. This map represents the dimension of the pillar structure for each discretized spatial location (the visible grid pattern visible in the phase maps of Fig. 11) along the metalens surface. The calculated phase maps can be seen in Fig. 12. Based on the structural map, the final metalens (as seen on Fig. 9) was designed in Lumerical FDTD.

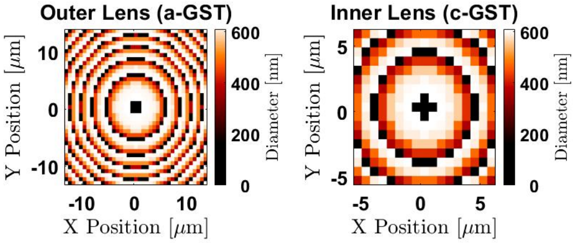

Fig. 12 | Structural maps. The above figure highlights the pillar diameter for each position on the metalens surface.

The full 3D simulation of the metalens employed an identical setup as used in the simulation of the unit cell, but with PML in all directions. The results of two metalens simulations (a-GST and c-GST) is shown in Fig. 13. The results of the full metalens simulations shows a clear intensity modulation as the GST phase is switched between a-GST and c-GST. The lower intensity in the c-GST phase is attributed to the relatively larger extinction coefficient. To verify the intensity modulation at various crystallization levels of GST, the Lorentz-Lorenz model from effective medium theory was employed.[12] For the intensity modulation demonstration, crystallization levels of 25%, 50%, and 75% was used (Fig. 14).

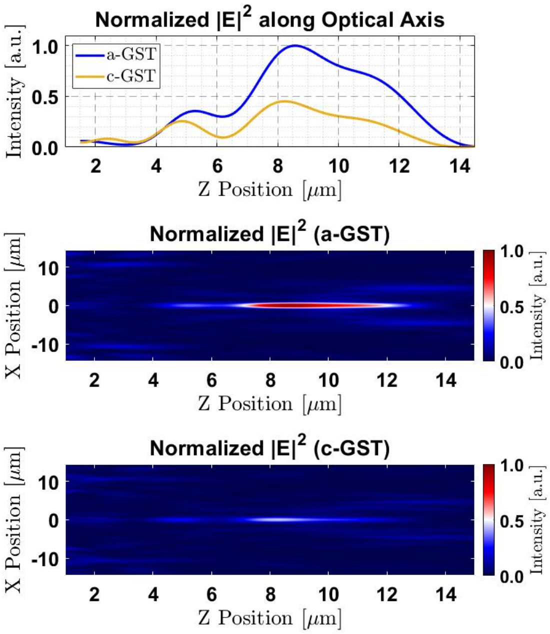

Fig. 13 | Simulated metalens intensity profile. The top figure illustrates the metalens intensity profile along the z-axis (optical axis) at x = 0 μm. Intensity peaks in the a-GST phase occurs at ~5.3 μm and ~8.6 μm. The peaks are slightly shifted to ~4.9 μm and ~8.2 μm in the c-GST phase. The figure also includes the simulated intensity along the $x - z$ plane for a-GST (middle) and c-GST (bottom).

As the crystallization ratio of the GST is increased, there is a clear intensity attenuation along the optical axis.

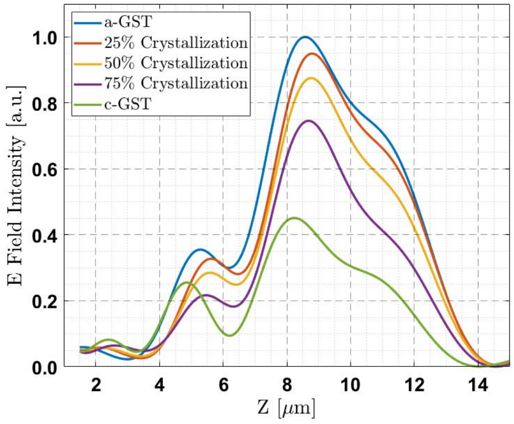

Fig. 14 | Simulated intensity modulation. The figure shows a continual intensity attenuation as the crystallization increases. In addition, a lateral shift in the two intensity peaks are also observed. An intensity modulation of ~43% is seen between the highest intensity peak in a-GST and c-GST.

However, this intensity attenuation effects both focal points simultaneously, and therefore did not show a tunable focus point as was predicted in Fig. 8. In addition, the two focal point locations show a deviation from design (5 μm and 10 μm). This error is possibly the result of phase error introduced by the phase profile discretization.[3] Furthermore, given the sharp phase gradient in the design do to due relatively short focal points, the design may be more sensitive to discretization and 8 levels may not be appropriate. It has been shown[3, 13] for metalens designs with short foci having sharp phase profiles, where dissimilar unit cells are placed next to each other, the coupling between the unit cells can reduce the diffraction efficiency and lower focusing power of the lens.

Extension Results and Discussion

Under normal incidence of light, the original structure is polarization-insensitive due to the rotational symmetry of the circular pillar structure.[3] In the extended analysis, this rotational symmetry will be broken by introducing an elliptical pillar unit cell structure (Fig. 15) in lieu of the circular pillar structure.

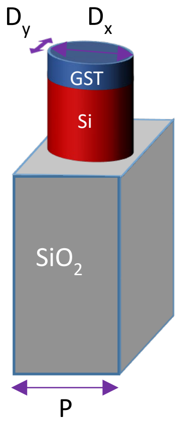

Fig. 15 | Elliptical unit cell. The proposed structure with short (D_y) and long (D_x) axis. The structure is 830 nm in height with 20 nm GST layer. In the final metalens design, the short and long axis of the structure is aligned with the x- and y-axis of as seen in Fig. 8.

Given this broken symmetry, the metalens should display different optical responses depending on the incident light polarization. If the elliptical structure is treated as a truncated waveguide, it stands to reason that orthogonal polarization along the two axis (D_x and D_y) of the new structure will experience different effective indices. As such, each unit cell with an elliptical pillar induces a polarization dependent phase delay onto the transmitted light.[14] It is important to note however, the azimuthal angle (orientation) of the new structure is not changed. Therefore, linear polarized light along the two axes will not be modified.[14] The same principle of structural birefringence have previously been employed in vortex metalenses to generate light with angular momentum.[15] Furthermore, with the additional degree of structural freedom (short and long axes) it should be possible to improve the total transmission efficiency of the unit cell across the full structural sweep range – a clear improvement from the transmission results shown in Fig. 10.

Similar to the original design procedure, the optical response of the new unit cell structure was extracted from FDTD simulations under x-polarized plane wave illumination. However, the parameter sweep was conducted for various axial dimensions of the elliptical pillar at 1550 nm. Thus, unlike the previous results, the optical response of the new structure (Fig. 16) was optimized at one wavelength.

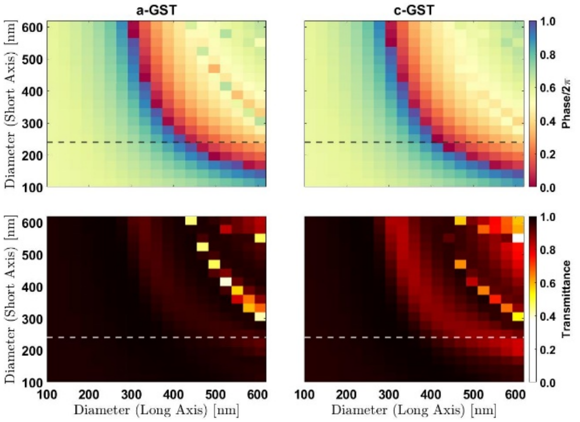

Fig. 16 | Parameter sweep of the elliptical unit cell. The left column represent the normalized phase (top) and transmittance (bottom) for amorphous GST. The right column represent the normalized phase (top) and transmittance (bottom) for crystalline GST. The parameter sweep was executed at a wavelength of 1550 nm. The dotted horizontal lines represent the optical response with a short axial (D_y) diameter of 240 nm. The provided results are for a unit cell period of 650 nm.

As seen from the results, by increases the total height of the pillar to 830 nm (keeping the GST layer at 20 nm), and reducing the period to 650 nm, a 2π phase response with an extremely high-level of transmission is feasible. This is a noticeable improvement from the previous design. Furthermore, from previous discussion on Huygens's based phase delay mechanism, the high transmission displayed by the new unit cell structure is characteristic of Huygen's based nanoantennas. This suggests both truncated waveguide and Huygen's nanoantennas mechanisms can play a role in the optical response of the new unit cell. In addition, geometrical phase cannot play a significant role in this structure as the azimuthal orientation of the unit cell was not altered. The subsequent design of the new metalens was conducted with the short axis (D_y) of the structure fixed to 240 nm. This dimension was chosen based on two criteria: high transmission and 2π phase response.

Following the same design procedure as before, the full metalens structure was created in Lumerical FDTD. Given the asymmetric nature of the new unit cell structure, a total of four (x- and y-linear polarized incidence illumination for both a-GST and c-GST) simulations were run. The results of which can be seen in Fig. 17 (x-polarization) and Fig. 18 (y-polarization).

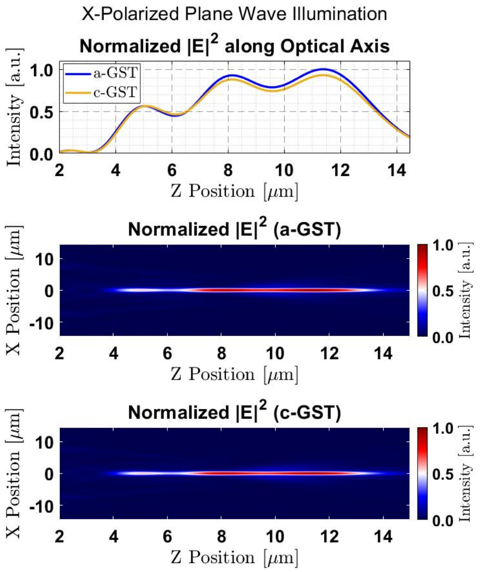

Fig. 17 | Simulated metalens intensity profile (x-polarization). The top figure illustrates the metalens intensity profile along the z-axis (optical axis) at x = 0 μm. Intensity peaks in the a-GST/c-GST phase occurs at ~5 μm, ~8.2 μm and ~11.4 μm. The figure also includes the simulated intensity along the $x - z$ plane for a-GST (middle) and c-GST (bottom).

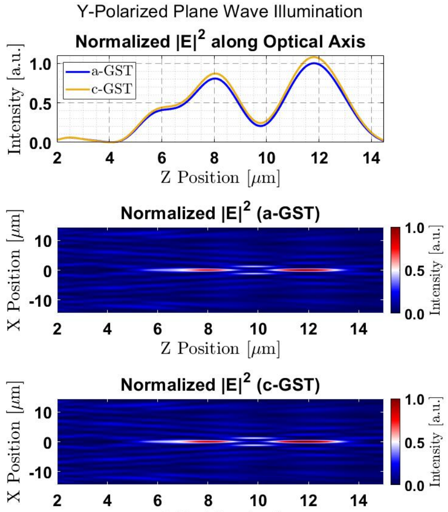

Fig. 18 | Simulated metalens intensity profile (y-polarization). The top figure illustrates the metalens intensity profile along the z-axis (optical axis) at x = 0 μm. Intensity peaks in the a-GST/c-GST phase occurs at ~8 μm, and ~11.8 μm. The figure also includes the simulated intensity along the $x - z$ plane for a-GST (middle) and c-GST (bottom).

For both linear polarization of incident light, the altered metalens exhibit minimum intensity modulation across the optical axis. This suggests that there is minimum light interaction with GST layer. Otherwise, the intensity would show a stronger modulation due to higher absorption in the c-GST phase. Additionally, taking the intensity results from Fig. 17 and Fig. 18 together, the designed focal points near 5 μm and 10 μm seems to be present, however anomalous peaks present at ~8 μm and ~12 μm have unresolved these intensity peaks. Furthermore, the anomalous peaks are polarization-insensitive, thus cannot be due to waveguiding effects. Based on these results, the broken symmetry of the unit cell structure has introduced a Huygen's based phase delay mechanism[8] that have resulted in the integration of an additional phase profile on the already spatially multiplexed metalens surface. As before, to investigate the modulation contrast as a function of GST crystallization, the Lorentz-Lorenz model was used. The generated data for both polarizations can be seen in Fig. 19 below.

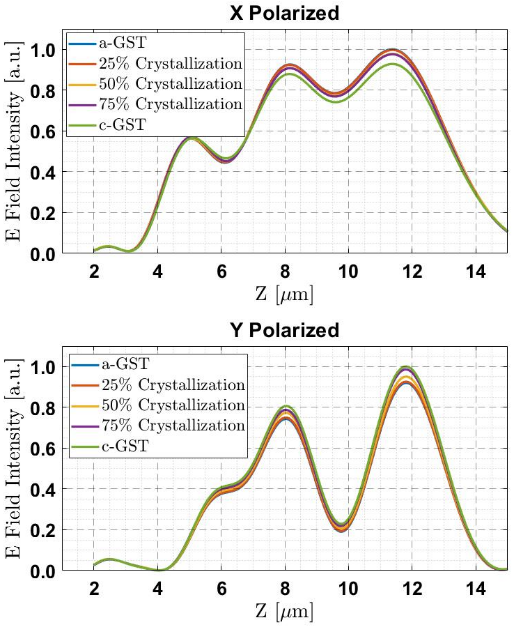

Fig. 19 | Intensity modulation for altered metalens design. Minimal intensity modulation is observed for incident plane wave of x- and y-polarization. In the case of x-polarization, the intensity decreases as the crystallization ratio increases. However, for the y-polarization case, the intensity is observed to increase with the increase in crystallization ratio. An intensity modulation between ~7% is possible for both polarizations.

From the modulation data, it is observed that modulation contrast remains the same for both polarizations. However, the modulation direction are in complete contrast between the x- and y-polarized incident light. A possible reason for this behavior might be due to differing diffraction efficiencies between the two polarizations. It is possible that in the case of y-polarization, there is a high degree of light diffraction to nonzero order. This undesired diffraction of light can result in a larger intensity reduction than what would be possible with purely material absorption in the c-GST phase.

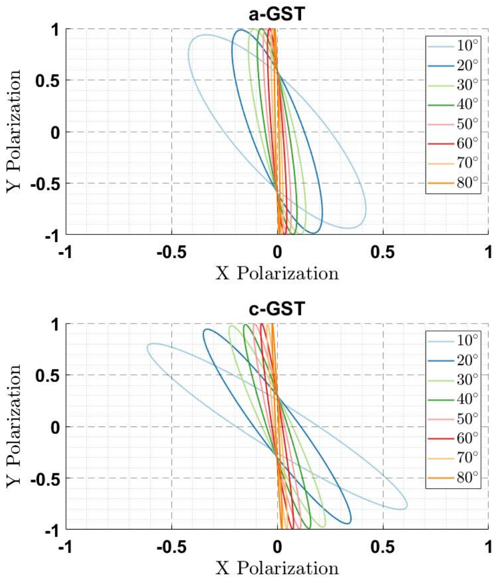

Fig. 20 | Simulated polarization ellipse. Polarization ellipse data for the 0th diffraction order for various linear polarization angles of incident light. The angles are defined with respect to the x-axis.

The effect of the metalens on the incident polarization of the light was characterized by simulating the polarization ellipse for various linearly polarized plane wave sources. The polarization ellipse (Fig. 20) provides a visual representation of the fraction of light contained in each orthogonal component. From the obtained results it is seen that for small angles, the phase transition between a-GST to c-GST provides a large modulation of the polarization ellipse. At a polarization angle of 10º, a polarization ellipse tilt angle difference of 16º was observed. Furthermore, the metalens is shown to induce a change in helicity of the incident light. This change is obtained at the cost of introducing a phase shift between the E_x and E_y components of the electric field. This behavior is most likely the structural birefringence introduced by the asymmetric unit cell structure.

Related Works

Numerous works have utilized the spatial multiplexing scheme for designing metalenses for various applications. Chen et al.[17] proposed replacing the array of microlenses and color filters from traditional CMOS image sensors with "full-color routing" metalens (Fig. 21). In this design, in contrast to multiplexing the entire metalens, the researchers judiciously multiplexed the unit cell with various resonator orientations to focus the primary colors (red, green and blue) to select locations on a plane parallel to the metalens surface. With such a design, the researchers claim the reproduce the vertical footprint of the CMOS sensor to just 0.6 μm – a drastic footprint reduction given the microlens array and color filter layers may be 1 μm to 10 μm in thickness. Arabi et al.[18] have also demonstrated multi-wavelength focusing using two spatial multiplexing schemes: large aperture division, and meta-atom interleaving (Fig. 22). Using this approach they were able to design a metalens that focuses incident light of two different wavelengths two the same focal points.

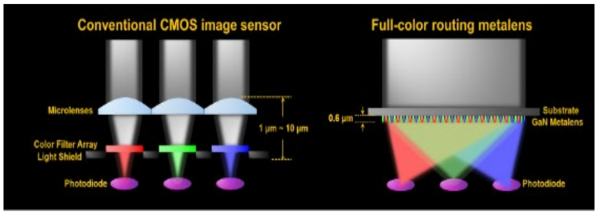

Fig. 21 | CMOS image sensor application of a metalens. A schematic of a metalens based color routing device for reduce the size and complexity of modern CMOS image sensors.[17]

Furthermore, the ideas proposed in this design may be generalized to more wavelength and provide a way forward for multifunctional metalens designs.

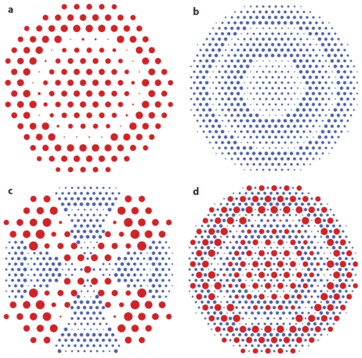

Fig. 22 | Multi-wavelength spatial multiplexing scheme. A) A schematic of a metalens designed to focus light at 1550 nm. B) A schematic of a metalens designed to focus light at 915 nm. C) Double wavelength metalens formed by aperture division spatial multiplexing, and D) by interleaving meta-atoms.[18]

Recently, Chang et al.[19] has demonstrated the 2D beam steering based on dielectric metalens integration on a switchable silicon micro -ring emitter array (Fig. 23). This technology has practical applications in free-space communication and LiDAR systems. By using Mach-Zehnder switches and micro-heaters, the light is routed to desired micro-ring emitters and the radiated light is focused at different position in free-space by the metalens. However, the addition of micro-heaters may cause thermal issues as the density of emitter are increased. Thus, micro-ring resonance tuning via PCM based evanescent coupling may be a possible alternative with the additional opportunity to expand on the steering capabilities by introducing a metalens design with similar capabilities as discussed in this report.

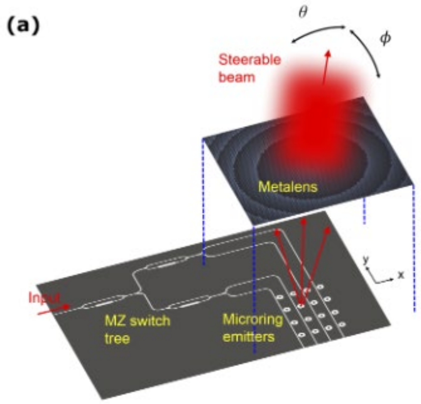

Fig. 22 | Multi-wavelength spatial multiplexing scheme. A schematic of a beam steering platform based on metalens integration on top of silicon photonic based switchable micro-ring emitter.[19]

Summary and Future Direction

A detailed investigation of a tunable bifocal metalens design proposal was conducted. The proposed design uses phase change material (GST) and spatial multiplexing to establish intensity modulated bi-focal functionality. The design was further extended by introducing asymmetric subwavelength resonators to the metalens. This alteration resulted in a polarization sensitive metalens with multiple encoded phase profiles on one metalens. In practice, this stacked phase profile behavior resulted in focal points with polarization insensitivity and sensitivity. Furthermore, the extended design was able to alter the helicity of the incident light while providing a possibility to alter the transmitted polarization of light via phase transitioning the thin GST layer. The lens design has potential applications in optical communication, high-resolution manufacturing, optical spectroscopy, imaging, optical tweezers, and holography.

In future studies alternative low-loss PCMs such as GSST may be considered to improve the focusing intensity while provided the necessary modulation and polarization conversion. In the extended design, the azimuthal orientation of the unit cells were not explored. The addition of this capability will utilize the geometrical phase delay mechanism which could provide additionally functionality for the proposed design. Furthermore, through the cascade of multiple metalenses, the focusing point of the light may be modulated at any location in 3D space by virtue of three mechanisms of phase delay: propagation phase, geometrical phase, and Huygen's nanoantennas.

Device Fabrication and Characterization

The proposed metalens design is fabricated on a fused silica substrate. This substrate was prepped with acetone, piranha and plasma ashing cleaning process to eliminate any organic contaminants. Then plasma-enhanced chemical vapor deposition (PECVD) is used to deposit the amorphous silicon (a-Si) layer to the desired thickness (300 nm and 830 nm). Afterwards, RF sputtering is used to deposit the 20 nm GST layer. Positive electron beam resist is spin coated and a soft bake is applied to reduce the solvent concentration. Once the resist has sufficiently cooled and rehydrated, a thin water-soluble anti-charging conductive polymer such as aquaSave™ [14] is applied. The pattern is written using electron-beam lithography, and the charging layer is removed with water. Subsequently, the pattern is developed using resist developer, and blown dry with nitrogen. Next, and aluminum is deposited by thermal evaporation in order to create a hard mask for etching. Life-off is carried out by submerging the substrate in solvent stripper.[16] Due to the high aspect ratio of the unit cell structures, inductively coupled plasma-reactive ion etching (ICP-RIE) is used. Once the etching is done the aluminum is removed.

The device characterization is done using a 1550 nm laser source (either a supercontinuum laser such as NKT "Super K" or a tunable laser such as Santec TSL series). The laser beam is collimated and passed through a linear polarizer. For imaging a high numerical aperture objective lens along with a tube lens and an InGaAs camera is used. A linear polarizer is also placed between the objective lens and the tube lens as an analyzer to image different polarization components of the transmitted light.

References

1. Tseng, M. L. *et al.* Metalenses: Advances and Applications. *Advanced Optical Materials* **6**, 1800554 (2018).
2. Lenses | Boundless Physics. https://courses.lumenlearning.com/boundless-physics/chapter/lenses/.
3. Li, S. *et al.* Active all-dielectric bifocal metalens assisted by germanium antimony telluride. *J. Phys. D: Appl. Phys.* **52**, 095106 (2019).
4. Yu, N. *et al.* Light Propagation with Phase Discontinuities: Generalized Laws of Reflection and Refraction. *Science* **334**, 333–337 (2011).
5. Aieta, F. *et al.* Aberration-Free Ultrathin Flat Lenses and Axicons at Telecom Wavelengths Based on Plasmonic Metasurfaces. *Nano Lett.* **12**, 4932–4936 (2012).
6. Kamali, S. M., Arbabi, A., Arbabi, E., Horie, Y. & Faraon, A. Decoupling optical function and geometrical form using conformal flexible dielectric metasurfaces. *Nat Commun* **7**, 11618 (2016).
7. Ding, F., Pors, A. & Bozhevolnyi, S. I. Gradient metasurfaces: a review of fundamentals and applications. *Rep. Prog. Phys.* **81**, 026401 (2017).
8. Lin, D., Fan, P., Hasman, E. & Brongersma, M. L. Dielectric gradient metasurface optical elements. *Science* **345**, 298–302 (2014).
9. Decker, M. *et al.* High-Efficiency Dielectric Huygens' Surfaces. *Advanced Optical Materials* **3**, 813–820 (2015).
10. Mandal, A., Cui, Y., McRae, L. & Gholipour, B. Reconfigurable chalcogenide phase change metamaterials: a material, device, and fabrication perspective. *J. Phys. Photonics* **3**, 022005 (2021).
11. Karvounis, A., Gholipour, B., MacDonald, K. F. & Zheludev, N. I. All-dielectric phase-change reconfigurable metasurface. *Appl. Phys. Lett.* **109**, 051103 (2016).
12. Aspnes, D. E. Local-field effects and effective-medium theory: A microscopic perspective. *American Journal of Physics* **50**, 704–709 (1982).
13. Yang, Y. *et al.* Dielectric Meta-Reflectarray for Broadband Linear Polarization Conversion and Optical Vortex Generation. *Nano Lett.* **14**, 1394–1399 (2014).
14. Arbabi, A., Horie, Y., Bagheri, M. & Faraon, A. Dielectric metasurfaces for complete control of phase and polarization with subwavelength spatial resolution and high transmission. *Nature Nanotech* **10**, 937–943 (2015).

15. Ma, Y., Rui, G., Gu, B. & Cui, Y. Trapping and manipulation of nanoparticles using multifocal optical vortex metalens. *Sci Rep* **7**, 14611 (2017).
16. Khorasaninejad, M. *et al.* Achromatic Metasurface Lens at Telecommunication Wavelengths. *Nano Lett.* **15**, 5358–5362 (2015).
17. Chen, B. H. *et al.* GaN Metalens for Pixel-Level Full-Color Routing at Visible Light. *Nano Lett.* **17**, 6345–6352 (2017).
18. Arbabi, E., Arbabi, A., Kamali, S. M., Horie, Y. & Faraon, A. Multiwavelength metasurfaces through spatial multiplexing. *Sci Rep* **6**, 32803 (2016).
19. Chang, Y.-C. *et al.* 2D beam steerer based on metalens on silicon photonics. *Opt. Express, OE* **29**, 854–864 (2021).